Molecular Crystals and Liquid Crystals Incorporating Nonlinear Optics

Publication details, including instructions for authors and subscription information:
http://www.tandfonline.com/loi/gmcl17

Holographic Gratings in Diacetylene Single Crystals

Hans-Dieter Bauer [a] , Thomas Vogtmann [a] & Markus Schwoerer [a]

[a] Physikalisches Institut and Bayreuther Institut für Makromolekülforschung (BIMF), Universität Bayreuth, P.O. Box 101251, D-8580, Bayreuth, Federal Republic of Germany

Version of record first published: 04 Oct 2006.

To cite this article: Hans-Dieter Bauer , Thomas Vogtmann & Markus Schwoerer (1990): Holographic Gratings in Diacetylene Single Crystals, Molecular Crystals and Liquid Crystals Incorporating Nonlinear Optics, 183:1, 421-437

To link to this article: http://dx.doi.org/10.1080/15421409008047481

Mol. Cryst. Liq. Cryst., 1990, vol. 183, pp. 421–437
Reprints available directly from the publisher
Photocopying permitted by license only

Printed in the United States of America

HOLOGRAPHIC GRATINGS IN DIACETYLENE SINGLE CRYSTALS

HANS-DIETER BAUER, THOMAS VOGTMANN, AND MARKUS SCHWOERER
Physikalisches Institut and Bayreuther Institut für Makromolekülforschung (BIMF), Universität Bayreuth, P.O. Box 101251, D-8580 Bayreuth, Federal Republic of Germany

Abstract Holographic gratings have been produced in macroscopic TS6 diacetylene single crystals via UV-photopolymerization. These gratings could be shown to be high efficient volume phase gratings with homogeneous absorption. Some diffraction characteristics significantly depend on the geometry of the write /read situation: Both the crystal anisotropy and the spatial anisotropy of the solid-state polymerization can influence the diffraction behavior. In this paper we discuss the effects of birefringence on the diffraction properties as well as some simple models which are a first approach to describe the phenomena observed in terms of reaction kinetics. As a result we give an estimate of the kinetic chain length during the induction period of the reaction.

INTRODUCTION

Diacetylenes

The 1,4-polyaddition of diacetylenes is the very example of a topochemical solid-state reaction. Monomer crystals of many diacetylene compounds can be quantitatively transformed into macroscopic polymer single crystals by applying pressure, heat or radiation, like UV light, x- or γ-rays:

$$\left(R - C \equiv C - C \equiv C - R \right)_n \xrightarrow[UV/kT]{} \left(\begin{matrix} R \\ | \\ C = C = C = C \\ | \\ R \end{matrix} \right)_n$$

In many fields of research these compounds are subject to intense work[1,2]. In this paper we deal with the diacetylene investigated best: TS6, where

$$R = -CH_2 - O - SO_2 - \text{Ø} - CH_3$$

The conversion curve obtained from thermal polymerization (Fig. 1) starts with a flat increase of polymer content with time (induction period) and then enters a

phase where the reaction rate rapidly grows (autocatalytic region). The reason for this behavior is the "mismatch" of monomer stacking distance in b-direction between monomer and polymer crystal. This mismatch causes a certain strain, which, in the course of the reaction, supports further polymerization and should result in longer polymer chains than at the beginning of the reaction[3,4].

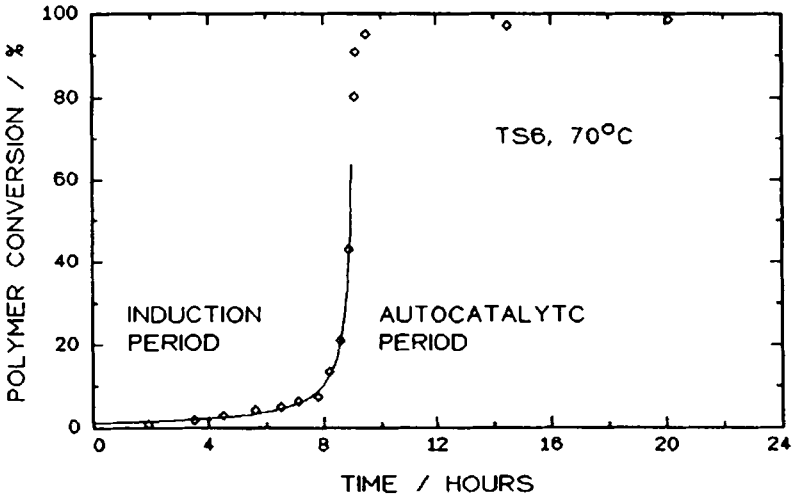

FIGURE 1 Time-conversion curve of TS6, polymerized at 70°C, with a hyperbola fitting the data points < 50% conversion.

The intermediate states of TS6 during this reaction are well known except for the structure of the chain ends[5,6,7,8,9,10]. Once terminated, at room temperature chains are believed not to become active again. Unlike other polydiacetylenes, the poly-TS6 chains are insoluble in all organic solvents. For poly-4BCMU[11] and TS12[12] chain lengths of some hundred to some thousand monomer units have been found.

Optical properties

The optical properties refractive index, n_0, and absorption coefficient, α_0, change extremely during the reaction. In former experiments we showed that both quantities don't vary linearly with polymer content P[13]. Phenomenologically, the functions which fit P and n_0 best during the induction period (and only in this period !) are

$$P(t) = a/(b - t) - c \qquad \text{for } P < 0.5 \tag{1}$$

$$n_0(P) = u[\,1 - v \exp(-wP)\,] \tag{2}$$

with a=0.128h, b=9.2h, c=0.0021 and u=1.674, v=0.068, w=23.275.
n_0 approximately represents the main value n_y (see experimental section).

Diacetylene crystals as a holographic recording material

In previous papers[14] we showed that these crystals can be used to record high efficiency volume phase gratings, yielding up to 63% efficiency and showing a clear Bragg behavior, causing sharp angular selectivity halfwidths $\Delta\Theta$ down to 0.12°. An analysis using the well-known coupled-wave approach established by Kogelnik[15], Magnusson and Gaylord[16,17], gave refractive index modulation amplitudes ranging from 0.001 to 0.01 and let us understand the dependence of $\Delta\Theta$ on sample thickness and UV penetration depth.

THEORY

Recording process

Two fully coherent plane waves of equal amplitude and wavelength λ_w superposed symmetrically in an isotropic medium of thickness d (Fig. 2a) give an interference pattern

$$I(x) = I_0[1 + \varkappa \cos(Kx)] \tag{3}$$

with the contrast $\varkappa$,

$$\varkappa = \begin{cases} 1 & \text{for H-mode polarization: scalar grating} \\ \cos(2\Theta_w) & \text{for E-mode polarization: vector grating} \end{cases}$$

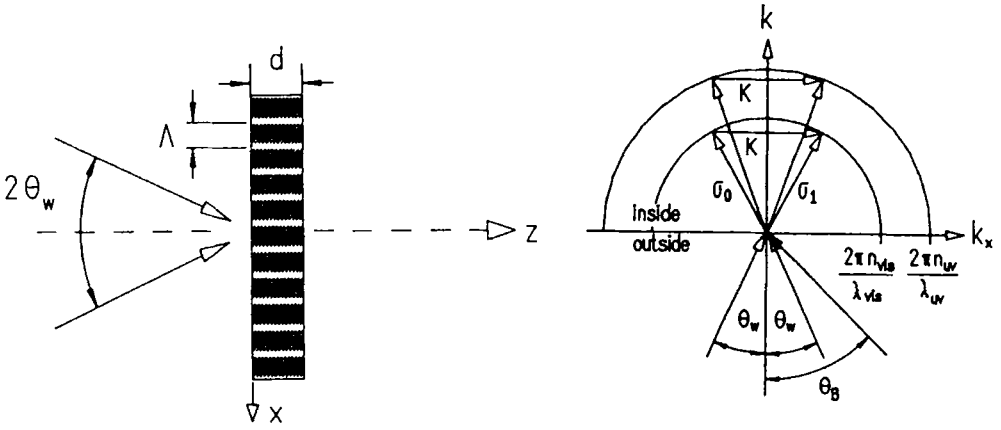

FIGURE 2 a) Writing a grating by superposing two plane waves symmetrically on the sample, yielding a fringe distance Λ. b) k-space representation of recording and readout process with different wavelengths. For abbreviations see text.

where Θ_w is the angle of incidence inside the medium. The grating spacing Λ is given by the grating vector $\mathbf{K}$ using

$$\Lambda = 2\pi/|\mathbf{K}| \tag{4}$$

or, like it can be seen from the k-space representation in Fig. 2b, by

$$\Lambda = \lambda_w/(2\sin\Theta_w) \tag{5}$$

Readout process

Applying only one of the two plane waves (the "reference wave") on the holographic grating leads to a reconstruction of the other one (the "object wave") if the correct angle of incidence has been chosen equal to the writing angle Θ_w. If another wavelength λ is used for the reconstruction, the correct readout angle Θ is given by

$$\Theta = \arcsin(\lambda\sin(\Theta_w)/\lambda_w) \tag{6}$$

This situation is shown in Fig. 2b. The most important feature of a grating is its efficiency η, which is the ratio of diffracted intensity and incident intensity,

$$\eta = I_{dif}/I_{inc} \tag{7}$$

This quantity usually is a function of hologram thickness d, modulation amplitudes of refractive index, n_1, and of absorption coefficient, α_1, overall absorption α_0 and angle of incidence, Θ. The relation between η and these values is established by the coupled-wave approach first introduced by Kogelnik[15], Magnusson and Gaylord[16,17]. The grating is represented by a Fourier series in n and α, which is restricted to cosine terms in the case of the symmetric writing process applied here:

$$n(x,z) = n_0 + \exp(-z/l)\sum_{h=1}^{\infty}\hat{n}_h\cos(hKx) \tag{8}$$

$$\alpha(x,z) = \alpha_0 + \exp(-z/l)\sum_{h=1}^{\infty}\hat{\alpha}_h\cos(hKx) \tag{9}$$

where an exponential decrease of the modulation according to the finite penetration depth l of the UV light is assumed. A dependence of n_0 or α_0 on z shall be neglected. The propagation vectors $\boldsymbol{\sigma}_i$ of the diffraction orders i emanating from the grating are coupled to the one of the incident light, $\boldsymbol{\sigma}_0$, by

$$\boldsymbol{\sigma}_i = \boldsymbol{\sigma}_0 + i\mathbf{K} \tag{10}$$

Kogelnik treated the case of pure cosine gratings (n_h, α_h = 0 for $h \geq 2$) and assumed only a first diffraction order (i = 1) to be present. For this situation the

analytical expression for the diffraction efficiency η can be given:

$$\eta(d) = \left[\sin^2\left(\frac{n_1 \pi d}{\lambda \cos\Theta}\right) + \sinh^2\left(\frac{\alpha_1 d}{2\cos\Theta}\right)\right] \exp\left(-\frac{\alpha_0 d}{\cos\Theta}\right) \qquad (11)$$

where d is the hologram thickness, Θ the angle of incidence, λ the readout wavelength and α_0 the overall absorption. For profiles n_1, α_1 not constant in z the corresponding average values have to be used. Magnusson and Gaylord generalized the problem on gratings of arbitrary profile and more than one diffracted wave. They arrived at a system of coupled differential equations, which we showed for our case can be simplified to yield a matrix equation

$$\mathbf{S}'(z) = \mathbf{M}\mathbf{S}(z) \qquad (12)$$

with the matrix **M** containing all the information on the n and α profile and on the geometry involved and the vector **S** whose elements are the field amplitudes of the different waves present. The solution is simply

$$\mathbf{S}(z) = \mathbf{S}(0)\exp(\mathbf{M}z) \qquad \eta_i(z) = S_i(z)S_i^*(z) \qquad (13)$$

This equation can be implemented on a computer to calculate efficiencies in a very quick way, especially necessary for fitting routines. For details see reference 13.

EXPERIMENTAL

The way to synthesize TS6 and to grow macroscopic diacetylene single crystals has been described elsewhere[18]. We used platelets, approx. 20 to 200µm thick and some mm^2 in area, cleaved from a parent crystal parallel to the (100) surface. For comparing the two different exposure geometries discussed below we split these platelets into two parts of nearly the same thickness and the same optical quality ("platelet pairs").

Writing was performed with either a cw HeCd laser (λ_w=325nm) or a XeCl excimer laser (λ_w=308nm). Readout was done with a HeNe laser (λ=633nm).

The setup we used has been described thoroughly in previous papers[14,19]. Here we want to point the reader's attention to the two kinds of exposure geometry given in Fig 3. The "b$\parallel$" orientation means that UV and VIS waves are polarized perpendicularly to the plane of incidence and that the polymer growth direction b is parallel to the grating fringes produced. The "b$\perp$" case is given, when UV and VIS polarizations and the b direction are lying in the plane of incidence, thus b is perpendicular to the fringes. Analyzing a holographic grating with a readout beam polarized perpendicularly to the b-axis leads to diffraction efficiencies more than one order of magnitude smaller and not well reproducible.

TS6 belongs to the monoclinic space group $P2_1/c$ and, therefore, is a biaxial crystal. With the help of a comfortable spindle-stage method[20] the position of the

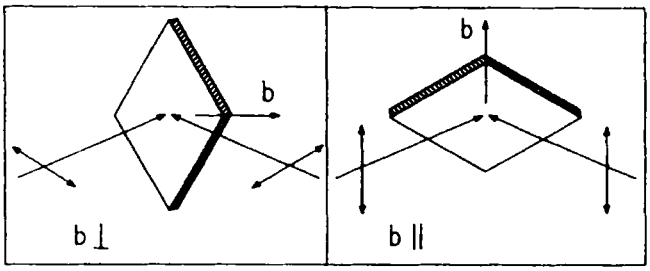

FIGURE 3 The two orientations of crystal axis b and polarizations relatively to one another.

two optical axes relative to the crystal axes have been determined together with the main refractive index values for 633nm (Fig. 4):

$$n_x = 1.570 \pm 0.002 \qquad n_y = 1.609 \pm 0.002 \qquad n_z = 1.70 \pm 0.01 \qquad (14)$$

These values showed no dramatic changes within the whole visible spectrum so that we assume $n_x < n_y < n_z$ for the near UV region, too.

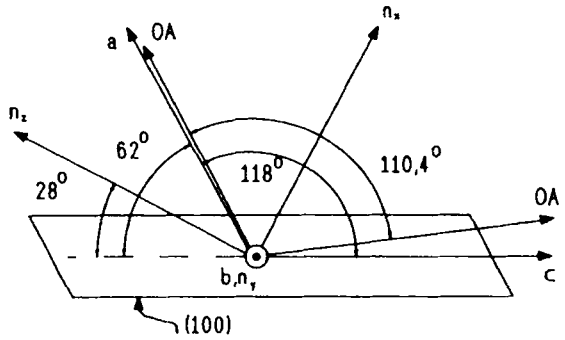

FIGURE 4 Orientation of crystal axes, indicatrix and optical axes relatively to one another. (100) is the surface shown unshaded in Fig. 3.

RESULTS

Birefringence effects

When writing a grating in b|| orientation one gets maximum diffraction for red light at the Bragg angle, also after rotating the sample around the z-axis for 180°. When the same writing process is done with unpolarized UV light, the pattern of Fig. 5 is observed: The usual Bragg peak is accompanied by a second one; it can be found on the same side of the main peak for +1st and -1st order. After a z-rotation of the

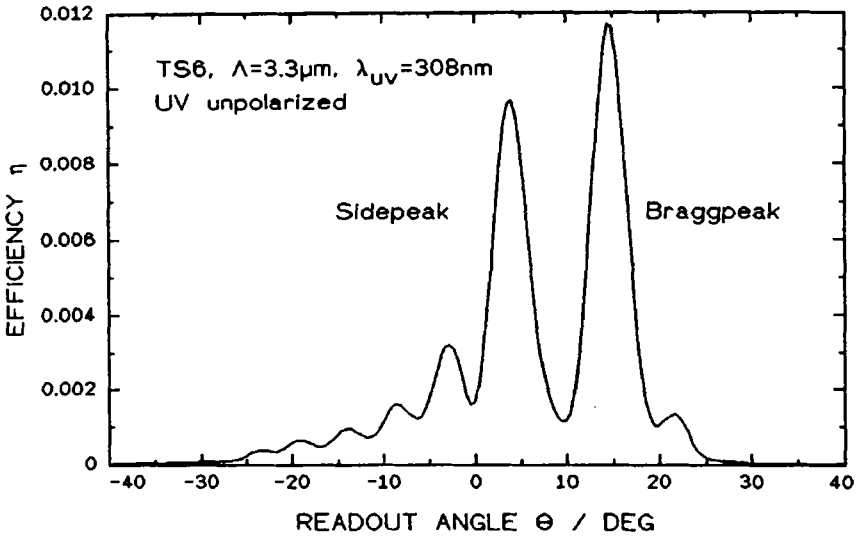

FIGURE 5 First order diffraction efficiency versus angle of incidence for a grating written with unpolarized UV light (λ_w=308nm, Λ=3.3μm) and read with VIS light (λ=633nm).

sample for 180° both extra peaks are found on the other side of the Bragg peaks.

A grating which has been written in b⊥ orientation and analyzed with red light shows two satellite peaks at each Bragg peak. Both are located in the same angular

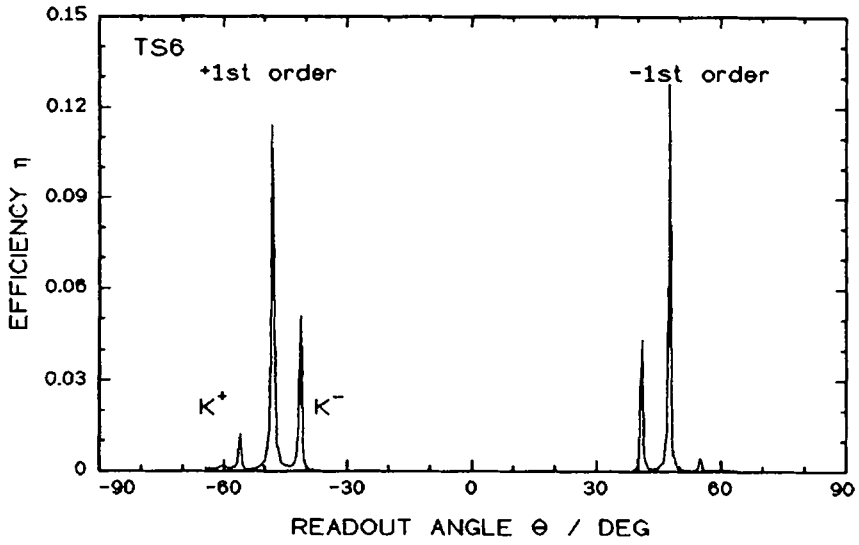

FIGURE 6 ±1st order diffraction efficiency of a grating written with λ_w=325nm in b⊥ orientation. Braggpeaks and sidepeaks according to the grating vectors **K**, **K**$^+$, and **K**.

distance from the main peak (Fig. 6). The distance to the main peak is the same for both satellites. Their position is not influenced by a sample rotation of the kind mentioned above.

Influence of orientation geometry on efficiency values

In a series of experiments "platelet pairs" were used for recording holographic gratings of different orientation but same exposure. Some of these pairs had been thermally "prepolymerized" to a certain degree before. Though large statistical errors - obviously due to optical inhomogeneities - the following trend could be noticed:

In the average the η values of the b $\parallel$ case exceeded the η values of the b $\perp$ case. This trend became clearer with increasing prepolymer content and with decreasing grating distance (Fig. 7).

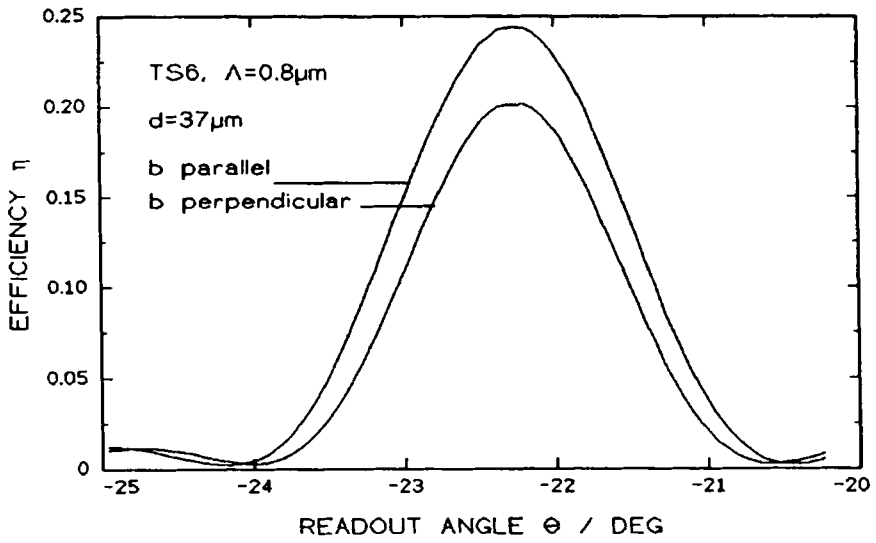

FIGURE 7 Efficiency of the two gratings recorded in one "platelet pair" and applying different writing geometry. Both samples have undergone the same exposure.

Thermal development of holographic gratings

In another series of experiments we used fresh samples to write holographic gratings with Λ = 3.3μm, which then were further thermally polymerized in the absence of UV light. During the induction period of the reaction the diffraction of these gratings was observed. A remarkable difference between both orientations could be seen:

In the b $\parallel$ case the first diffraction order showed a slight increase, a second order, if present at all, hardly showed any growth (Fig. 8). Higher orders usually did not appear or ranged hardly above stray light in intensity.

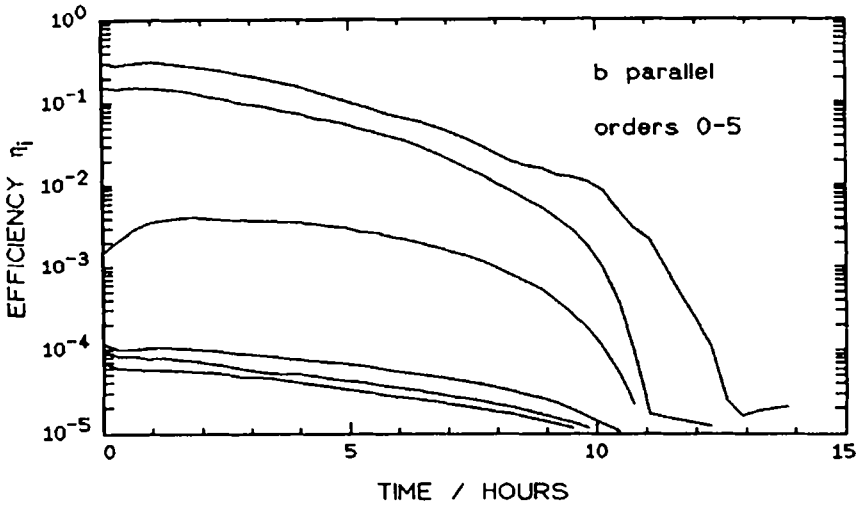

FIGURE 8 Thermal development of a holographic grating: Λ=3.3μm, T=70°C, b|| orientation.

In the b⊥ case the second order showed a dramatic increase which covered one or two orders of magnitude. A 3rd, 4th and even 5th order appeared in the course of the reaction (Fig. 9). The 1st order approximatly behaved like in b|| case.

In both figures the maximum efficiency of the order of interest is depicted, i.e. each of them was measured at the according Bragg angle.

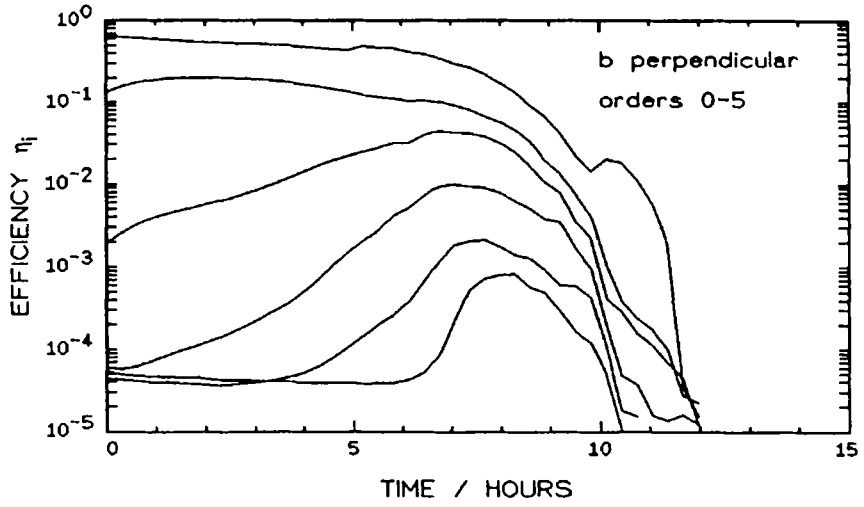

FIGURE 9 Thermal development of a holographic grating: Λ=3.3μm, T=70°C, b⊥ orientation. Thickness and exposure of this sample approximately the same than of the one shown in Fig. 8.

The decrease of the "0th order", the transmitted light, is due to an increase in absorption. Crystals entering the autocatalytic region become nearly totally opaque for 633nm light, which can be seen by the breakdown of all the curves given in Figs. 8/9.

Our main interest was pointed towards the appearance of higher diffraction orders in the b⊥ case. Some quantitative results are:

Absolute values:

1) The maximum efficiency values of the 1st diffracted order, η_1^{max}, always surpassed or at least were found to equal the starting values, η_1^{st} (Fig. 10).
2) The higher diffraction orders i = 2, 3, and 4 reached 0.14, 0.04 and 0.01 as maximum values η_i^{max}. As can be seen from Fig. 10, an increase in η_1^{st} led to an increase of η_i^{max} , too.
3) The starting efficiency of the second order, η_2^{st}, also shows an increase with increasing η_1^{st}. At very low η_1^{st} the values < 0.1% may be partially due to stray light.
4) The maximum efficiency η_2^{max} also clearly grows with growing η_1^{max} (Fig. 11).

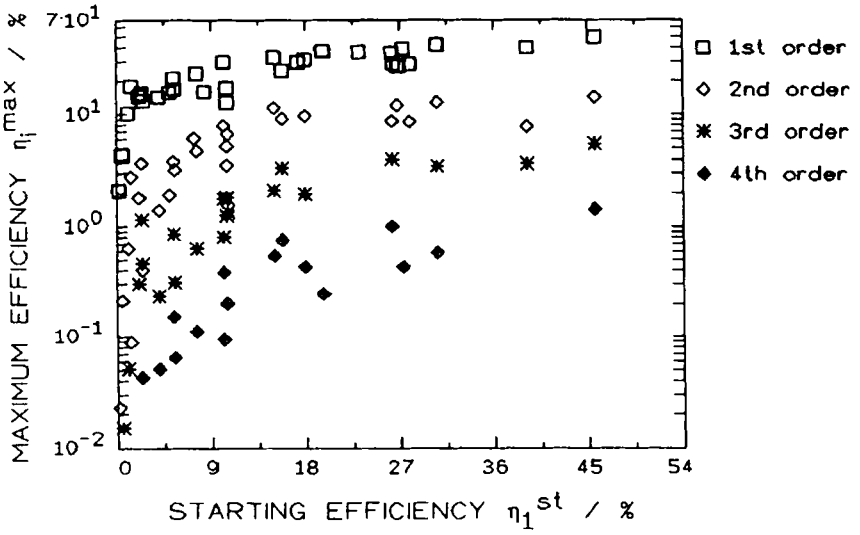

FIGURE 10 The maximum diffraction efficiencies of order 1-4 reached during a thermal development versus starting efficiency of the first order. Sample thickness ranged from 100 to 200μm typically. Λ=3.3μm, b⊥ orientation.

Relative values:

1) The quotient of maximum efficiency during thermal development and starting efficiency, η_1^{max}/η_1^{st}, is a measure for the degree of growth of the first order. This quotient can reach values up to 10 at very low η_1^{st}. For higher starting efficiencies this value decreases rapidly and for η_1^{st} > 0.2 no increase can be observed anymore.
2) The ratio η_2^{max}/η_2^{st} is found to be very high for small η_1^{st} values, decreasing rapidly for higher η_1^{st}.

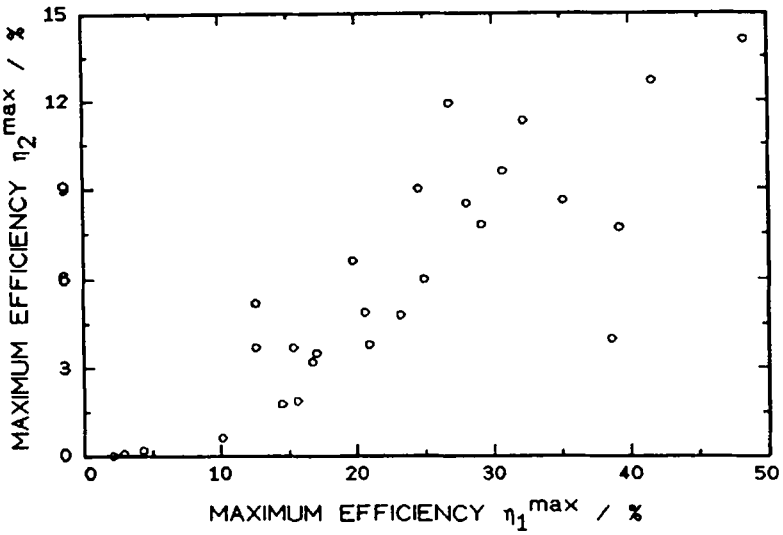

FIGURE 11 Maximum efficiency observed in for the second diffraction order versus the one observed for the first order in the same experiment.

Time to reach the maximum value:

1) The time, at which the maximum value η_1^{max} is reached, t_1^{max}, also strongly depends on the starting efficiency η_1^{st}. The smaller η_1^{max} is, the closer to the "autocatalytic edge" is this time (Fig. 12).

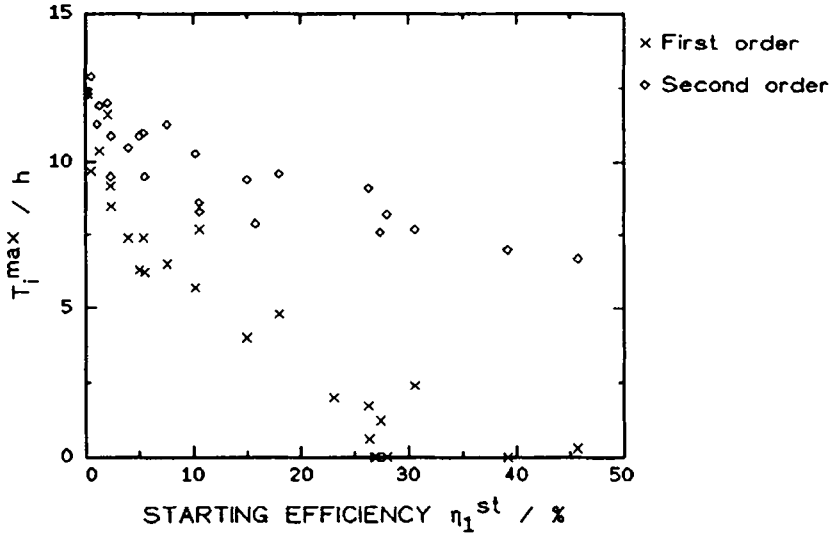

FIGURE 12 Time to reach the maximum efficiency during a thermal development as it has been measured for the first and second diffraction order, versus the starting efficiency of the first order.

2) For the second order this dependence is much weaker, but the t_2^{max} values also tend to get smaller with increasing η_1^{st} (Fig. 12).

DISCUSSION

k-space scenarios

The two write/read geometries can be eplaind by the k-space representations in Fig. 13. In b|| orientation both writing beams travel in a plane spanned by the two optical axes and are polarized perpendicularly to this plane and parallel to the b (= n_y -) axis, hence their polarization is not altered. The refractive index for both is n_y and a readout beam polarized in H-mode, too, gives the usual diffraction pattern like in an isotropic medium.

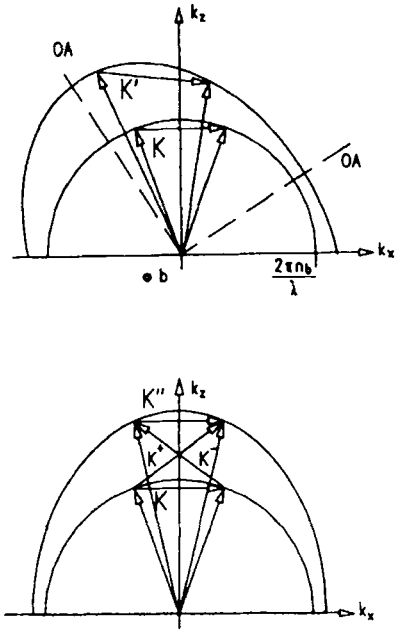

FIGURE 13

k-space representations for writing a holographic grating in b|| orientation (above) or in b⊥ orientation (below).

In the case b|| the "normal" grating vector **K** is produced, like it would have been in an isotropic medium. By rotating the UV polarization into the plane of incidence, a tilted grating **K'** is produced.

In the case b⊥ four waves interfere to produce three gratings, a "symmetric" one, **K**, and two which are tilted relatively to one another, $\mathbf{K}^+$ and $\mathbf{K}^-$.

When UV light is present which is polarized in the plane of incidence, the refractive index is a function of the angle of incidence and both UV waves will undergo different diffraction according to n_1 and n_2. This results in a tilted grating **K'**.

When read with red light of H-mode, the Bragg condition is fulfilled for an angle different from the "original" one.

The case of b⊥ orientation is characterized by a special symmetry:
Both writing waves enter the crystal symmetrically to the plane spanned by the optical axes. Both beams undergo birefringence, splitting up into two waves polarized perpendicularly to one another. Therefore, four plane waves of different polarization are present in the medium to interfere with each other. This results in the formation of four gratings, two of which are identical (**K**) and the other two ($\mathbf{K}^+$ and $\mathbf{K}^-$)

are tilted with respect to **K** in opposite directions. When read with VIS light, the Bragg condition is fulfilled successively for each of these three gratings. The intensity of the satellite peaks depends on the degree of birefringence, i.e. their intensity is the smaller, the smaller Θ_w is: We could observe these peaks at Λ=0.4 and 0.8μm, but not at Λ=3.3μm.

Chain length, polymer profile, and grating profile

A model describing the spatially inhomogeneous reaction kinetics of diacetylenes must take into account a kinetic chain length L, which depends on the polymer conversion P. The monomolecular reaction in a simple homogeneous situation then is given by

$$dP/dt \sim L(P)(1 - P) \tag{15}$$

For the experiments described in 4.2. L can be assumed constant during the exposure time, because only very little conversion takes place. And for all experiments descri-

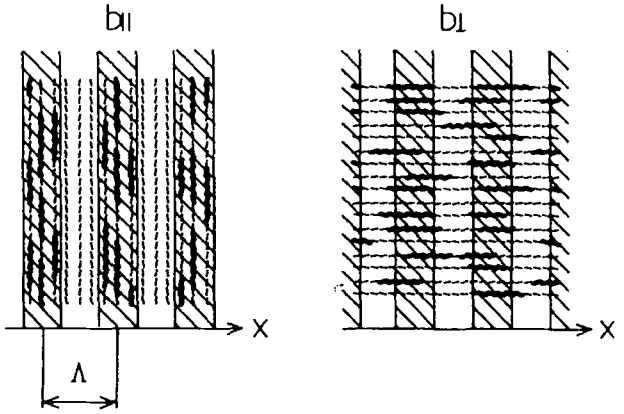

FIGURE 14 Microscpic model to understand the interaction of the two characteristic lengths Λ and L: The two geometries investigated change the angle between chain growth direction and grating fringes.

bed the factor (1 - P) will be dropped, because they have been carried out in the low conversion regime of the induction period and because saturation effects would have affected the development experiments of both orientations. For the two orientations different situations must be investigated, corresponding to the different interaction of the two characteristic lengths Λ and L (Fig. 14):

$$b \parallel: \quad dP/dt \sim L(P)\cos^2(\pi x/\Lambda) \tag{16}$$

Here a polymer molecule grows parallel to the fringes, contributing with its whole chain length L to the polymer growth at point x, where it has been initiated. In the

other case a chain initiated in x contributes to the polymer growth in the whole interval [x-L/2, x+L/2]:

$$b\perp: \quad dP/dt \sim \int_{x-L/2}^{x+L/2} \cos^2(\pi x'/\Lambda)dx' \tag{17}$$

Integration of both equations yields (for an exposure time t_e):

$$P_{\parallel}(x,t_e) \sim L(P)t_e\cos^2(\pi x/\Lambda) \tag{18}$$

$$P_{\perp}(x,t_e) \sim [\, L/2 + \Lambda/(2\pi)\left(\cos(2\pi x/\Lambda)\sin(\pi L/\Lambda)\right)]t_e \tag{19}$$

So the chain growth "smears out" the photoproduct distribution for a certain amount in the second case. This effect should be the stronger, the more L/Λ approaches 1. For $L = \Lambda$ no grating and, therefore, no diffraction should be observable anymore.
For the quotient of both polymer modulations we get the ratio δ:

$$\delta = \Delta P_{\perp}/\Delta P_{\parallel} = \sin(\pi L/\Lambda)/(\pi L/\Lambda) \tag{20}$$

This quantity now is independent of exposure time and independent of contrast ! In good approximation Δn ($= 2n_1$) can be assumed to be proportional to ΔP. The analysis of efficiency values from the experiments described above then should render a good estimate of δ, and, therefore, $L(P)$, possible. Nevertheless, some corrections have to be done before: Different reflectivity of the sample for both orientations has to be taken into account as well as the intensity that went into the formation of satellite peaks. Unfortunately this only can be done when knowing about refractive index values in the UV region. The same corrections have to be made for the read process. We used a set of n_{uv} values approx. 5% higher than the VIS values. An eventual anisotropy of he polymer yield was neglected.

The resulting δ values range between 0.95 and 0.85 for fresh samples and tend to decrease with increasing prepolymer content. For samples prepolymerized 5-6 hours (3-4% polymer) we found δ ranging between 0.8 and 0.65. These values would indicate chain lengths of 0.15 to 0.4µm or 300 to 800 repeat units.

In the case of thermal development another onset has to be made:
Starting from a profile $P_0(x,t=0)$ the development in $b\parallel$ orientation is ruled by

$$dP_{\parallel}(x,t)/dt \sim L(P_{\parallel}(x,t)) \tag{21}$$

If one assumes a linear dependence of L on P, $L(P) = L_0(1 + \xi P)$, then

$$P_{\parallel}(x,t) \sim (1/\xi)[\, (1 + \xi P_0(x))\exp(L_0\xi t) - 1\,] \tag{22}$$

which represents a profile both growing exponentially in average polymer content and

modulation. For a quadratic dependence, $L(P) = L_0(1 + \xi P^2)$, one gets

$$P_{\parallel}(x,t) \sim (1/\sqrt{\xi})\tan\left[L_0\sqrt{\xi}\, t + \arctan(\sqrt{\xi}\, P_0(x))\right] \quad (23)$$

For b⊥ orientation we have

$$dP_{\perp}(x,t)/dt \sim \int_{x_L}^{x_R} dx' \quad (24)$$

where x_L and x_R are functions of $P(x)$! Because of the dependence of $L(P)$, the interval $[x_L, x_R]$ is of variable length and has not to be symmetric: the point x can be reached from chains initiated to its left or to its right; the maximum distance it can be reached from is dependent on P. This integral is only numerically solvable.
A polymer profile will cause a refractive index profile $n(x)$ due to the dependence of n on P:

$$n(x,P) = n_0(P) + \sum_h n_h(P)\cos(hKx) \quad (25)$$

For the simple relation given as equation (2) this would give

$$n_h(P) = 2uv\exp(-wP)\sinh(-wP_h) \quad (26)$$

as long as $n_h \ll n_0$.

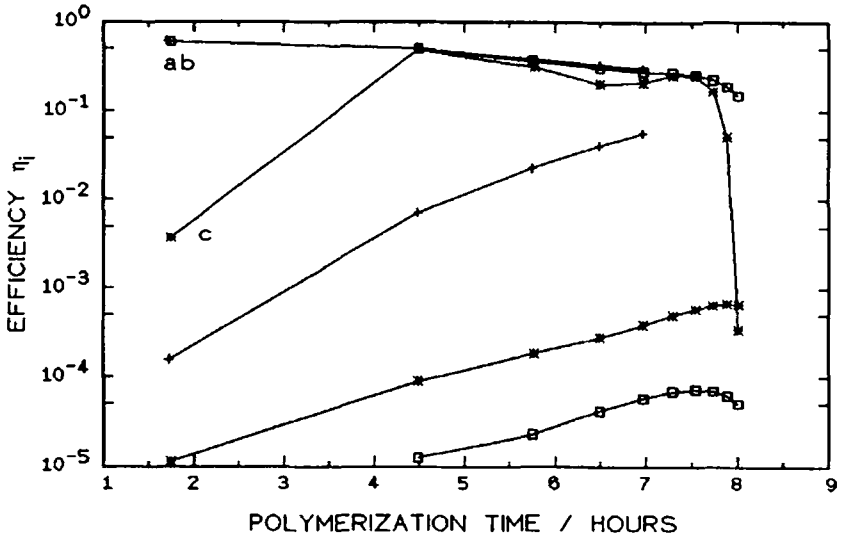

FIGURE 15 Simulation of a thermal development of the 1st and 2nd order via (26) with different parameter sets for the linear model: a) (squares) L_0=0.025μm, L_{10}=1.0μm, P_0=0.001; b) (crosses) L_0=0.01μm, L_{10}=0.5μm, P_0=0.001; c) (asterisks) L_0=0.01μm, L_{10}=0.5μm, P_0=0.0025.

We tried to fit an index profile to some of the measurements of the kind given in Fig. 9. using the formalism given in (12) and (13). By changing the signs of the Fourier coefficients we found these gratings not to vary remarkably, i.e. the diffracted waves nearly behave uncoupled. So we simulated thermal development kinetics according to (24), Fourier-analyzed the polymer profiles, and transformed the n_h obtained by (26) into efficiencies via (11). The parameters we changed were the starting chain length, L_0, which can be assumed very short[21], and the starting modulation, P_0. The quantity mentioned last has to be chosen small, so that no periodic behavior of the first order efficiency occurs. Then the chain length at 10% conversion, and therefore ξ, was varied. Figs. 15 and 16 show different results for different parameter sets. Both linear and quadratic model give higher diffraction orders. The experiments show a scenario which seems closer to the one suggested by the quadratic model. Especially a behavior similar to the one shown in Fig. 12 can be observed. The simulations that we have performed until now indicate polymer chain lengths of 1μm or more at 10% conversion.

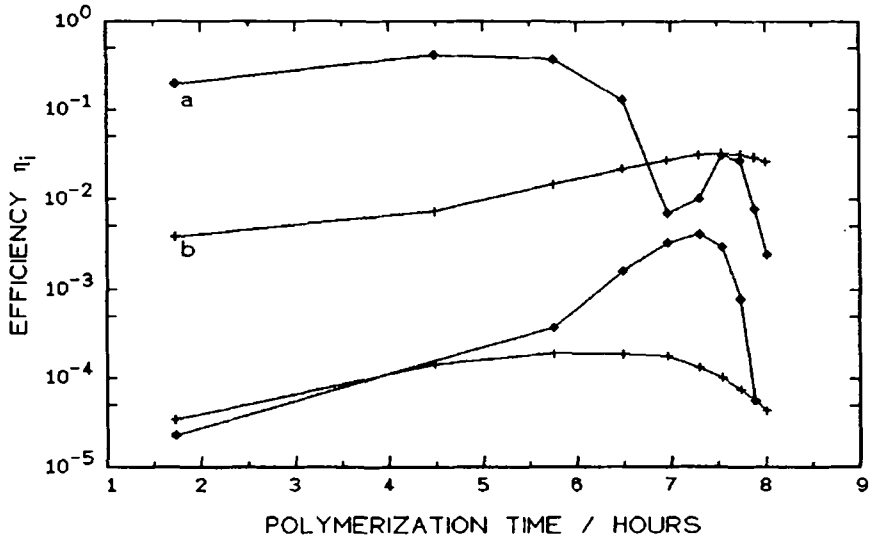

FIGURE 16 Simulated efficiencies of the 1st and 2nd diffraction order for a thermal development following (26) and assuming the quadratic model: a) (asterisks) L_0=0.01μm, L_{10}=1.0μm, P_0=0.0005; b) (crosses) L_0=0.01μm, L_{10}=0.5μm, P_0=0.0001.

CONCLUSIONS

Though the analysis of diffraction efficiencies is not a precision method for the determination of polymer molecule length, we could show that phenomena observed during our work can be attributed to the anisotropic growth of such polymer chains. The factors that hinder us from a better quantitative understanding of the effects

explained above are the lack of UV refractive index values and their dependence on polymer content as well as the variable optical quality of our samples which only permit a single use experiment. The microscopic models used to describe the built-up of higher orders during a thermal development may not be perfect, but give a first insight in a possible way to understand this phenomenon.

The estimates we gave for the polymer chain length nevertheless are in the range of values measured for other diacetylenes with the help of more common and reliable methods[11,12].

Acknowledgement

We thank Irene Müller for growing the excellent crystals, G. Denninger, G. Sauer and H. Hereth for technical assistance and O. Medenbach, Universität Bochum, for the indicatrix measurements and helpful discussions. This work has been supported by the Deutsche Forschungsgemeinschaft, SFB 213 / B2.

References

1 H.J. Cantow, editor, "Polydiacetylenes", Adv. Polym. Sci. 63 (Springer, Berlin 1984).
2 D. Bloor and R.R. Chance, editors, "Polydiacetylenes", NATO ASI Series E 102 (Nijhoff, Dordrecht 1985).
3 R.H. Baughman, J. Chem. Phys. 68, 3110 (1978).
4 R.H. Baughman and R.R. Chance, J. Chem. Phys. 73, 4113 (1980).
5 M. Schwoerer, R.A. Huber, and W. Hartl, Chem. Phys. 55, 97 (1981).
6 W. Hartl and M. Schwoerer, Chem. Phys 69, 443 (1982).
7 H. Niederwald and M. Schwoerer, Z. Naturforsch 38a, 749 (1983).
8 H. Gross, H. Sixl, S.F. Fischer, and E.W. Knapp, Chem. Phys. 84, 321 (1984).
9 W. Neumann and H. Sixl, Mol. Cryst. Liq. Cryst. 105, 41 (1984).
10 R. Müller-Nawrath, R. Angstl, and M. Schwoerer, Chem. Phys. 108, 121 (1986).
11 G.N. Patel, R.R. Chance, and J.D. Witt, J. Chem. Phys. 70, 4387 (1979).
12 G. Wenz and G. Wegner, Makromol. Chemie Rapid Commun. 3, 231 (1982).
13 T. Vogtmann, H.-D. Bauer, I. Müller, and M. Schwoerer, in J. L. Bredas, editor, "Conjugated Polymeric Materials: Opportunities in Electronics, Optoelectronics, and Molecular Electronics", NATO ASI Series, submitted, to be published 1990.
14 H.-D. Bauer, T. Vogtmann, I. Müller, and M. Schwoerer, Chem. Phys. 133, 303 (1989).
15 H. Kogelnik, Bell Syst. Tech. J. 48, 2909 (1969).
16 R. Magnusson and T.K. Gaylord, J. Opt. Soc. Am. 67, 1165 (1977).
17 R. Magnusson and T.K. Gaylord, J. Opt. Soc. Am. 68, 1777 (1978).
18 G. Wegner, Z. Naturforsch. 24b, 824 (1969).
19 B.E. Kohler, H.-D. Bauer, Bern E. Kohler, W. Güttler, and M. Schwoerer, Chem. Phys. Lett. 125, 251 (1986).
20 O. Medenbach, Fortschr. Miner. 63, 111 (1985).
21 P. A. Albouy, P. Keller, and J. P. Pouget, J. Am. Chem. Soc. 104, 6556 (1982).